Journal of Solid State Chemistry 183 (2010) 668–675

Contents lists available at ScienceDirect

Journal of Solid State Chemistry

journal homepage: www.elsevier.com/locate/jssc

Synthesis and crystal structure of $CuZrTiO_5$—A new crystal structure type

Ulrike Troitzsch [a], Andrew G. Christy [a,*], Anthony C. Willis [b], David J. Ellis [a]

[a] Research School of Earth Sciences, Australian National University, Canberra ACT 0200, Australia
[b] Research School of Chemistry, Australian National University, Canberra ACT 0200, Australia

ARTICLE INFO

Article history:
Received 7 August 2009
Received in revised form
23 December 2009
Accepted 9 January 2010
Available online 18 January 2010

Keywords:
$CuZrTiO_5$
Synthesis
Crystal structure
In_2TiO_5
Polyhedral distortion
Bond valence

ABSTRACT

A new compound, $CuZrTiO_5$, was synthesized as strongly pleochroic green crystals from the oxides between 995 and 1010 °C, 1 atm. Its crystal structure was determined by single crystal XRD, resulting in R ($F^2 > 2\sigma(F^2)$)=0.032 and wR (all data)=0.079). $CuZrTiO_5$ is orthorhombic, space group $P2_12_12_1$, a=3.5871(3) Å, b=6.6968(4) Å, c=14.6679(9) Å, V=352.35(4) Å^3, Z=4. The structure is topologically similar to In_2TiO_5 but differs in space group and cation coordination. $CuZrTiO_5$ has relatively regular TiO_6 polyhedra, but coordination is 7+1 for Zr, and 4+2 for Cu due to the Jahn–Teller effect. Ordering of the long Cu–O bonds causes reduction in symmetry relative to In_2TiO_5. Layers of Cu alternate with Ti+Zr on (001), giving rise to a distinct cleavage. Bond valence sums on Ti and Zr are far from ideal, which appears due to the limited ability of this structural topology to avoid close next-nearest neighbour distances.

1. Introduction

The compound $CuZrTiO_5$ was discovered as a by-product in sintering experiments in the ZrO_2–TiO_2 system, and represents the first ternary oxide in the Cu–Zr–Ti–O system. Hence, no previous literature is available on this compound.

The solid-state reaction of ZrO_2 and TiO_2 to form intermediate compounds with compositions ranging from $ZrTiO_4$ [1] to $ZrTi_2O_6$ [2] proceeds only very slowly at temperatures below 1200 °C, due to sluggish reaction kinetics and/or nucleation difficulties [3–5]. In order to accelerate the reaction rate, various fluxes such as water, ammonium carbonate, lithium molybdate mixtures, and copper oxide have been tried by the authors in the past [4–8]. In these previous studies, the addition of 5 to 10 wt% CuO to the ZrO_2–TiO_2 oxide starting mixes resulted in formation of the desired intermediate compounds even below 1200 °C at atmospheric as well as higher pressures, thus allowing for phase equilibrium studies, as well as the synthesis of targeted ceramic compositions in the ZrO_2–TiO_2 system at this relatively low temperature [4,5,8]. At elevated pressures (5–40 kbar), the CuO seemed to disappear from the samples during the experimental runs, leaving a white, pure ZrO_2–TiO_2 sample charge behind, making CuO the ideal flux as it extracts itself during synthesis by a process that is yet to be understood [8]. It is suspected that the Cu^{2+} reduced during these piston–cylinder apparatus runs and alloyed with the surrounding, sealed platinum capsule. In contrast to this, experiments that were conducted at atmospheric pressure, for example using pressed pellets without the need for Pt encapsulation, resulted in samples that contained a Cu-rich phase in addition to the targeted ZrO_2–TiO_2 phases (Fig. 1a). Optically, these samples showed a light green colour. Against expectations, the additional phase was not a quenched Cu-rich melt, but a crystalline, new inorganic phase: $CuZrTiO_5$. This study presents the synthesis and characterization of multigrain samples as well as single-crystals of $CuZrTiO_5$, and discusses the crystal structure of this material, which to the best of the authors' knowledge represents a new crystal structure type.

2. Experimental procedures

2.1. Synthesis

Experiments bracketing $CuZrTiO_5$ synthesis temperature: The starting mix was prepared from the oxides with equal molar amounts of ZrO_2, TiO_2, and CuO (Aldrich, $<5\,\mu m$, $>99.9\%$). All oxides were dried separately before weighing (CuO at 400 °C, ZrO_2 and TiO_2 at 1000 °C). About 30 mg of the mix was filled into 2 mm diameter platinum capsules, which were crimped shut and subjected to various temperatures (Table 1). The product phases were identified with X-ray diffraction, and selected ones analysed with scanning electron microscopy.

Pellets: The starting mix was prepared from the oxides with equal molar amounts of ZrO_2, TiO_2, and CuO (Aldrich, $<5\,\mu m$,

* Corresponding author. Fax: +61 2 6125 5544.
E-mail address: Andrew.Christy@anu.edu.au (A.G. Christy).

0022-4596/$ - see front matter © 2010 Elsevier Inc. All rights reserved.
doi:10.1016/j.jssc.2010.01.005

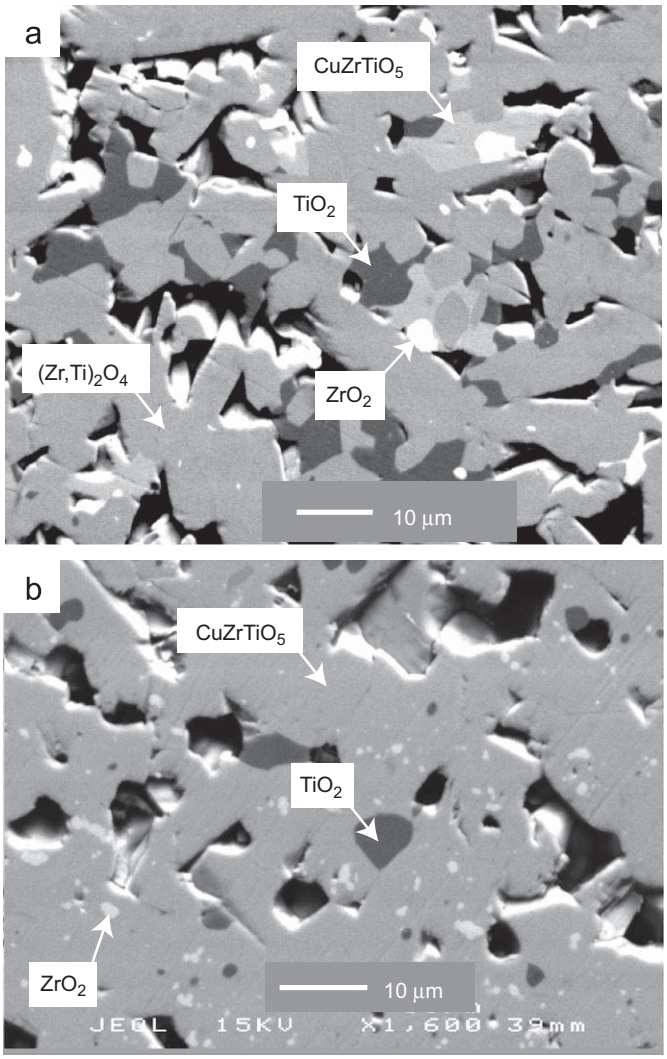

Fig. 1. (a) Backscattered electron micrograph of run product, showing copper-rich phase coexisting with Zr–Ti oxides and (b) micrograph of attempt to synthesise single-phase $CuZrTiO_5$, showing granular aggregate with small relict grains of TiO_2 and ZrO_2.

Table 1
Experimental details.

Sample	Starting mix (mol%)			T (°C)	t (h)	Product phases
	ZrO_2	TiO_2	CuO			
Experiments bracketing CZT synthesis temperature range (in Pt-capsules)						
ATMU147a	33.3	33.3	33.3	930	69	*T, Z,* C
ATMU214	33.3	33.3	33.3	980	24	*T, Z, C*
ATMU215	33.3	33.3	33.3	990	24	*T, Z, C*
ATMU216	33.3	33.3	33.3	995	65	*CZT, T, Z, C*
ATMU147b	33.3	33.3	33.3	1000	69	*CZT, T, Z*
ATMU144	49.5	49.5	1.0	1000	169	*T, Z, ZT, CZT*
ATMU217	33.3	33.3	33.3	1010	22	*CZT, T, Z*
ATMU 219	33.3	33.3	33.3	1015	23	*CT, T, Z*
ATMU218	33.3	33.3	33.3	1020	23	*CT, T, Z*
Pellets						
ATMU149	33.3	33.3	33.3	1000	73	*CZT, T, Z*
ATMU156	33.3	33.3	33.3	1000	55	*CZT, T, Z*
Single crystal experiment						
ATMU213	33.3	33.3	33.3	1000	149	*CZT, T, Z*

T: TiO_2 (rutile), *Z*: ZrO_2 (baddeleyite), *C*: CuO (tenorite) *ZT*: $(Zr,Ti)_2O_4$ (orthorhombic, ordered), *CT*: Cu_3TiO_4, *CZT*: $CuZrTiO_5$.

> 99.9%). All oxides were dried separately before weighing in (CuO at 400 °C, ZrO_2 and TiO_2 at 1000 °C). The oxide starting mix was then milled in ethanol for 30 min in a Rocklabs bench-top ring mill with zirconia head. Glycerol was added as binder, and the mixture pressed at 13 t for 5 min, dried at 40 °C, to form ~10 g pellets. Using a bench-top muffle furnace, these pellets were heated to 320 °C over the course of 3 h, then sintered at 1000 °C for 3 days at 1 atm. The pellet porosity was calculated using the final weight and calculated volume based on diameter and height.

Single crystals: Single crystals were synthesized using the same oxide starting mix as for the pellets. A Pt crucible with lid was filled with a 2 mm thick layer of CuO, then about 8 mm of starting mix, and another 2 mm thick layer of CuO. The CuO layers were added to minimize suspected Cu loss by evaporation or alloying with Pt. A few grains of $CuZrTiO_5$, harvested from previous multigrain experiments, were placed in the centre of the reactant layer to act as seeds. This assembly was then placed in a bench-top muffle furnace at 1000 °C, 1 atm, for 1 week. The resulting sample cake was carefully broken up, and individual crystals selected under the polarizing microscope for further investigation. There was no evidence whether the crystals used for this study grew from the seeds, or nucleated independently in the starting mix.

2.2. Scanning electron microscopy

Quantitative analyses were obtained with a JEOL JSM-6400 scanning electron microscope with attached Si(Li) detector, Link ISIS EDS, at 15 kV and 1 nA. Analyses were quantified using ZAF correction. Synthetic, homogeneous zirconolite ($CaZrTi_2O_7$) was used as standard for Zr and Ti, and tenorite (CuO) for Cu. The analyses have an estimated error of 0.5 wt% for each oxide.

2.3. Structure determination with single crystal X-ray diffraction

Two crystal structure determinations were carried out using different crystals. They resulted in the same crystal structure model and structural parameters within error, thus lending credibility to the refinement results of this study. Only one of these datasets is presented here. Images were measured at 295 K on a Nonius Kappa CCD diffractometer (Mo$K\alpha$, graphite monochromator, λ=0.71073 Å) and data extracted using the DENZO package [9]. The structure was solved by direct methods (SIR92) [10], and refined using the CRYSTALS programme package [11]. Figures showing crystal structure representations were generated with the programme CrystalMaker 7.2.4.

3. Results and discussion

3.1. Synthesis temperature of $CuZrTiO_5$

The reaction of the oxides to form $CuZrTiO_5$ was bracketed with a sequence of experiments ranging from 930 and 1020 °C (Table 1). Although the experiments reached only partial equilibrium, they identify and indicate the direction of reactions. Between 930 and 990 °C, only the initial phases from the starting mix, ZrO_2, TiO_2 and CuO, are present. $CuZrTiO_5$ appears at 995 °C as a product of the reaction:

$$ZrO_2 + TiO_2 + CuO = CuZrTiO_5 \quad (1)$$

and remains a stable phase in the assemblage until at least 1010 °C. The dominant Cu-phase at and above 1015 °C is the mixed oxide compound $Cu_3TiO_4 = Cu_2^{1+}Cu^{2+}TiO_4$ [12], which

indicates the increasing reduction of Cu^{2+} to Cu^{1+} at such temperatures, suggesting that the upper temperature limit for $CuZrTiO_5$ synthesis is controlled by a reaction such as

$$3CuZrTiO_5 = Cu_3TiO_4 + 3ZrO_2 + 2TiO_2 + 1/2O_2 \quad (2)$$

Thus, in our experiments, the synthesis of $CuZrTiO_5$ occurs only in the narrow temperature range between 995 and 1010 °C.

It has to be emphasized that Eqs. (1) and (2) describe the processes observed in the experiments, but do not necessarily correspond to stable reactions located at equilibrium temperatures. For example, binary compounds ranging in composition from $ZrTiO_4$ and $ZrTi_2O_6$ are stable phases in the ZrO_2–TiO_2 system in the temperature range discussed here, but form only if both flux and crystallization seeds are present in the starting mix due to sluggish reaction kinetics [4,5]. Since these phases were not the object of investigation of the experiments presented here (except for sample ATMU144), seeds were not added, and the compounds did not form, even though they should be part of the equilibrium assemblage. Thus, the co-existence of ZrO_2 and TiO_2, as observed in the experiments and suggested by reactions (1) and (2), is metastable only, and the phase assemblages presented in Table 1 cannot be used for the construction of equilibrium phase diagrams.

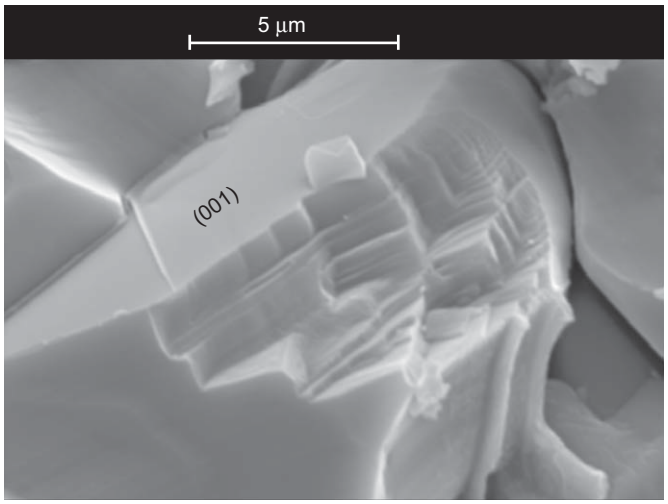

Fig. 2. Secondary electron micrograph of fractured $CuZrTiO_5$ grain, showing very distinct (001) cleavage.

3.2. Multigrain samples

For phase-characterization, the attempt was made to synthesise single-phase, polycrystalline samples of $CuZrTiO_5$ as pellets. The pellet samples sintered at 1000 °C are dark grey to black in colour, but the powdered material is bright green. The pellets are predominantly composed of $CuZrTiO_5$ grains of size $<20\,\mu m$ (Fig. 1b, Table 1), and contain a significant amount of relict inclusions of TiO_2 and ZrO_2, but no relict CuO. This indicates loss of CuO from the starting mix during sintering, which could have happened by either evaporation and/or by movement of CuO within the sample, possibly in the form of a CuO-rich melt. The amount of relict inclusions in the pellets is the reason for our attempt to grow single crystals for crystal structure investigations. Secondary electron images show that all $CuZrTiO_5$ grains in the pellet have at least one very distinct cleavage plane (Fig. 2),

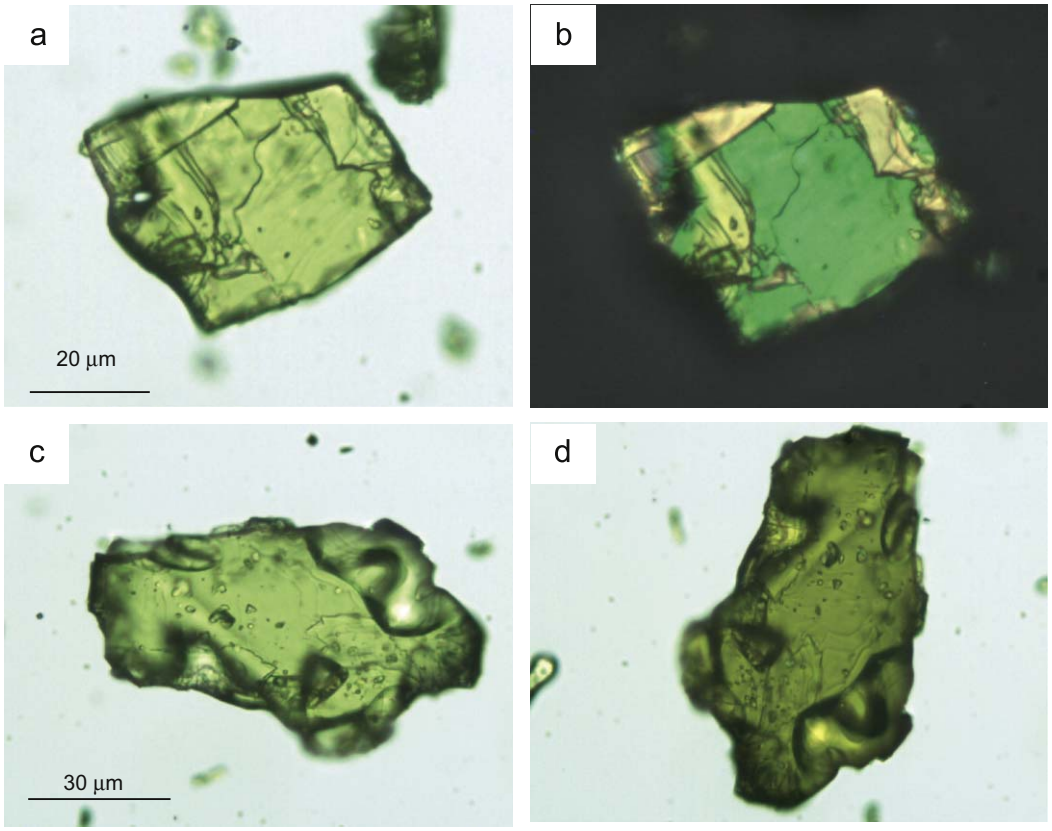

Fig. 3. Transparent green grain in optical microscope (a) shows cleavage cracks and between crossed polarisers shows birefringence colours (b). In plane-polarised light, $CuZrTiO_5$ shows pleochroism between a paler bottle green (c) and a darker green with a yellow/olive tint (d). (For interpretation of the references to colour in this figure legend, the reader is referred to the web version of this article.)

identified as the (001) plane in the crystal structure axial setting presented below. Cleavage steps estimated to be as thin as 250–500 Å were observed.

3.3. Single crystals and crystal structure

The single crystal preparation method resulted in $CuZrTiO_5$ grains ranging from 50–100 μm in size, which display the same distinct cleavage as those in the pellet samples (Fig. 3a, b). The grains are strongly pleochroic, with colours varying from yellow-green to bottle-green (Fig. 3c, d). A large crystal without any visible inclusions was selected under the optical microscope and used for crystal structure analysis.

Two independent single crystal structure determinations resulted in the same crystal structure model, and identical datasets within error. According to these, $CuZrTiO_5$ is orthorhombic, crystallizes in space group $P2_12_12_1$, and has the unit cell dimensions $a=3.5871(3)$ Å, $b=6.6968(4)$ Å, $c=14.6679(9)$ Å, $V=352.35(4)$ Å^3, $Z=4$ (Table 2). The Flack parameter was 0.43 ± 0.03, indicating substantial inversion twinning of the acentrosymmetric structure but not complete racemisation.

No isostructural phases were found in the Inorganic Crystal Structure Database [13]. However, the structure of $CuZrTiO_5$ does show a close similarity to that of In_2TiO_5 and In_2VO_5 (*Pmnb*, in the corresponding axial setting) [14,15]. In these compounds, all atoms lie on the mirror planes of that structure, whereas they are displaced along **a** in $CuZrTiO_5$, giving rise to strong violations of the glide plane absences and unambiguous acentric symmetry. The displacements result in changed cation and anion coordination numbers and bond valence distribution, as discussed at the end of this section, so $CuZrTiO_5$ is best regarded as belonging to a new structure type.

In $CuZrTiO_5$, all atoms occupy general positions (Table 3). The structure is composed of layers of edge- and corner-sharing CuO_6 octahedra parallel to (001), which alternate with double layers composed of ZrO_8 and TiO_6 polyhedra (Fig. 4). The ordering of cations into these (001) layers is likely to be the cause of the excellent cleavage on that plane displayed by $CuZrTiO_5$ crystals (Fig. 3). The Ti–Zr double layers are composed in turn of zigzag chains of edge-sharing TiO_6 octahedra along **a**, alternating with zigzag, edge-sharing ZrO_8 chains. Apart from the cation ordering, the topology of these Zr–Ti double layers (Fig. 4c) is reminiscent of distorted fluorite-type structures such as tetragonal zirconia [16].

All three types of cation polyhedra are significantly distorted, with distinctly unequal bond lengths and non-ideal bond angles (Tables 4 and 5, Fig. 5). Cu occurs in octahedral [4+2] coordination, with four oxygens forming an approximate square at similar distances between 1.915(4) and 2.029(4) Å, and two more distant ones on each side of the square at 2.591(4) and 2.565(5) Å at opposite apices (Fig. 5). This elongated coordination environment is a characteristic consequence of the Jahn–Teller effect frequently observed for Cu^{2+} with the electronic configuration $(Ar)t_{2g}^6 d_{z^2}^2 d_{x^2-y^2}^1$ [17,18]. Apart from such apical bond stretching, the octahedron is further distorted by tilting of the lengthened axis by about 20° with respect to the equatorial plane (Fig. 7), another common feature of such distorted CuO_6 octahedra [18,19].

Table 2
Crystal structure data and refinement results for $CuZrTiO_5$.

Crystal system	Orthorhombic
Space group	$P2_12_12_1$
Lattice parameters (Å)	$a=3.5871(3)$
	$b=6.6968(4)$
	$c=14.6679(9)$
Volume (Å^3)	352.35(4)
Z	4
Density (calculated) (g/cm^3)	5.328
Absorption coefficient (mm^{-1})	10.980
θ range (deg)	3.344–30.035
Crystal size (μm)	$10\times60\times70$
Total number of reflections measured	5421
Number of independent reflections	1022
Number of reflections with $F^2>2\sigma(F^2)$	932
Final R indices (all data)	$R=0.0358$, $wR=0.0792$
Final R indices (2σ cut-off)	$R=0.0319$, $wR=0.0765$
Flack parameter	0.43 (3)

Table 3
Atomic coordinates of $CuZrTiO_5$.

	x	y	z	U_{iso} (Å^2)	Occ	M	BVS
Cu	0.4996(2)	0.59953(12)	0.74592(5)	0.0104	1	4	2.01
Zr	0.07575(15)	0.34112(8)	0.59597(3)	0.0071	1	4	3.63
Ti	0.5886(3)	0.64208(14)	0.42604(6)	0.0064	1	4	4.31
O1	0.5693(11)	0.3451(6)	0.6888(2)	0.0085	1	4	1.89
O2	0.1004(12)	0.6371(6)	0.6494(3)	0.0107	1	4	1.96
O3	0.5777(13)	0.3840(6)	0.5160(3)	0.0086	1	4	1.88
O4	0.0872(12)	0.6459(7)	0.4643(3)	0.0126	1	4	2.18
O5	0.5972(13)	0.4405(6)	0.3405(3)	0.0093	1	4	2.03

U_{iso}: isotropic displacement factor, Occ: site occupancy, M: site multiplicity, BVS: bond valence sum.

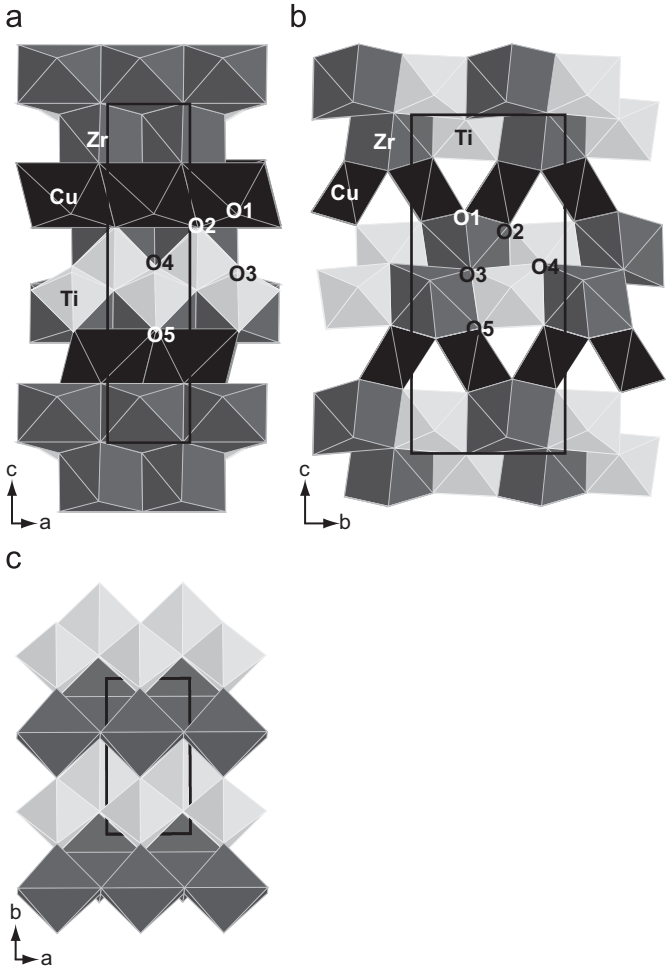

Fig. 4. Polyhedral diagrams of the $CuZrTiO_5$ structure: (a) view down [010], showing (001) layers of CuO_{4+2} polyhedra alternating with ZrO_8–TiO_6 double layers; (b) view down [100], with long Cu–O bonds not shown. CuO_4 squares form kinked corner-sharing chains, and the (Zr,Ti) double layers are seen to have edge-sharing chains of Zr and Ti polyhedra alternating along **b** and (c) view down [001] of a Zr–Ti double layer.

The TiO_6 octahedron is characterized by an off-centered Ti^{4+} ion that is displaced towards the O2–O5 edge, causing the opposite two Ti–O bonds to be significantly longer (2.146(4) and 2.175(4) Å) than all others (1.843(4)–1.884(4) Å) (Fig. 5). Off-centre distortions of octahedra containing d^0 transition metals like Ti^{4+} are not unusual. They are driven by a second-order Jahn–Teller effect which destabilises centrosymmetric coordination environments; the magnitude and direction of distortion are influenced by effects such as bond network, lattice stresses, and cation–cation repulsion [20,21]. In the case of $CuZrTiO_5$, Ti^{4+} is displaced towards one of the two unshared edges of the octahedron, away from the nearest neighbouring Ti^{4+} (at 3.165(2) Å) and Zr^{4+} (at 3.252(2) Å and 3.476(2) Å), suggesting that cation–cation repulsion is the main driving force behind this displacement. Zr occurs in [7+1] coordination, with seven Zr–O distances between 2.105(4) and 2.271(4) Å, and one at 2.810(4) Å (Fig. 7).

The bond valence method is a powerful way to assess the accuracy of interatomic distances, and also sources of local strain in a structure that may limit its stability. The technique and its applications are surveyed extensively in a monograph by Brown [22]. Bond valences were calculated using the relationship $R=R_0-b\ln s$ where R=cation–anion bond length, R_0=the bond length for unit bond valence, b=the constant 0.37 Å and s=bond valence, and the Brese and O'Keeffe values for R_0 (Cu – O=1.679 Å, Ti – O=1.815 Å, Zr – O=1.937 Å, In – O=1.902 Å) [23]. The bond valence sum (BVS) of 2.01 for Cu is close to ideal (Table 3), whereas BVS=4.31 at the Ti site indicates significant overbonding and that of 3.63 at the Zr site a similar degree of underbonding. This bond valence mismatch cannot be attributed to mixed cation occupancy on these sites, as this would put some of the larger cation on an already overbonded site and *vice versa*, rendering the BVS mismatch even worse. Hence, bond valence mismatch is a driving force for full cation order in this structure. Oxygen BVS also deviate from the ideal values, being 1.91, 1.98, 1.92, 2.18 and 2.05 for O1–O5, respectively.

The BVS for an atom increases if it moves away from the centroid of its coordination polyhedron, as a consequence of the distortion theorem [22]; the high BVS for Ti is evidently an instance of this effect, driven by cation–cation repulsion. It should be noted, however, that although the structure contains distances between edge-sharing cations that are short (shortest Ti···Ti=3.165 Å, Ti···Zr=3.252 Å, Zr···Cu=3.184 Å), they are not anomalously so compared to Ti···Ti=2.958 Å in rutile TiO_2, Zr···Zr=3.353 Å in baddeleyite ZrO_2, or Cu···Cu=2.900 Å in tenorite CuO. Similarly, the shortest O···O distance along the edge shared between TiO_6 polyhedra (O4···O4=2.502 Å) is not excessively so, and is close to the 2.530 Å shared edge in rutile. The BVS deviations in $CuZrTiO_5$ do not appear to be driven by specific repulsive interactions, but rather by the overall structural topology necessitating a large number of moderately short non-bonded distances.

The displacement parameters for some atoms in the structure are quite large and anisotropic (Tables 3–6). In particular, the long axis of the O4 ellipsoid points along the long bond to the underbonded Zr and perpendicular to the shorter, stronger bond to Ti (Fig. 7). The relatively elongated ellipsoid for Cu points along the long O5′–Cu–O2 axis of its coordination octahedron, as do those of the oxygens, suggesting that correlated displacement of these atoms keeps the overall BVS constant.

3.4. Powder versus single crystal diffraction pattern

A comparison between the measured powder X-ray diffraction pattern of $CuZrTiO_5$ (pellet sample ATMU149, crushed) and that calculated from the single-crystal structure determination is shown in Fig. 6. Although all major peaks are present in the sample pattern, some of them are significantly broadened and of lower intensity compared to the calculated pattern. The variation in peak width made it impossible to solve the structure by Rietveld refinement of the powder pattern.

We note that the $0\,0\,l$, $0\,k\,0$, $0\,k\,l$ and $h\,k\,0$ reflections in the powder pattern remain relatively sharp, while $h\,0\,l$ and $h\,k\,l$ are broadened. Similar anisotropic broadening has been observed in high-pressure neutron diffraction patterns of PbO, where a tetragonal-orthorhombic phase transition caused fine {110} twinning that left $h\,h\,l$ peaks sharp while broadening the rest [24]. In the case of $CuZrTiO_5$, retention of narrow $0\,k\,l$ peak widths would imply that d_{010}, d_{001} and α^* remain close to their ideal values, because the distortion of the structure involves only displace-

Table 4
Selected bond distances in Å in $CuZrTiO_5$.

Bond	Distance	Bond	Distance	Bond	Distance
Cu–O1	1.915(4)	Ti–O2	1.847(4)	Zr–O1	2.271(4)
Cu–O1′	1.919(4)	Ti–O3	2.175(4)	Zr–O1′	2.234(4)
Cu–O2	2.591(4)	Ti–O4	1.875(4)	Zr–O2	2.134(4)
Cu–O2′	2.029(4)	Ti–O4′	2.146(4)	Zr–O3′	2.156(5)
Cu–O5	2.022(4)	Ti–O4″	1.884(4)	Zr–O3	2.229(4)
Cu–O5′	2.565(5)	Ti–O5	1.843(4)	Zr–O3″	2.168(5)
				Zr–O4	2.810(4)
				Zr–O5	2.105(4)
av. Cu–O	2.174	av. Ti–O	1.962	av. Zr–O	2.263

Table 5
Selected bond angles in $CuZrTiO_5$.

Cu	Angle (deg)	Ti	Angle (deg)	Zr	Angle (deg)		Angle (deg)
O1′–Cu–O2	107.24(15)	O2–Ti–O3	179.38(17)	O1′–Zr–O3	117.05(15)	O2–Zr–O3″	92.37(15)
O1′–Cu–O2′	98.66(17)	O2–Ti–O4	98.4(2)	O1′–Zr–O5	73.26(16)	O2–Zr–O4	64.98(13)
O1′–Cu–O5	82.15(16)	O2–Ti–O4′	85.38(17)	O1–Zr–O1′	105.56(15)	O2–Zr–O5	131.94(15)
O1′–Cu–O5′	73.27(15)	O2–Ti–O4″	100.9(2)	O1′–Zr–O2	74.46(15)	O3″–Zr–O5	109.13(16)
O1–Cu–O1′	176.01(12)	O2–Ti–O5	100.27(17)	O1–Zr–O2	78.57(15)	O3′–Zr–O3″	112.09(16)
O1–Cu–O2	74.87(15)	O3–Ti–O4″	79.22(19)	O1–Zr–O3	116.90(16)	O3–Zr–O3′	72.06(14)
O1–Cu–O2′	84.12(17)	O3–Ti–O4	81.15(19)	O1′–Zr–O3′	170.63(14)	O3–Zr–O3″	71.84(13)
O1–Cu–O5	95.10(16)	O3–Ti–O4′	94.07(16)	O1–Zr–O3′	170.90(14)	O3″–Zr–O4	61.31(14)
O1–Cu–O5′	104.63(15)	O3–Ti–O5	80.27(16)	O1–Zr–O3′	70.24(14)	O3′–Zr–O4	62.71(14)
O2′–Cu–O5	179.03(18)	O4′–Ti–O5	174.27(17)	O1′–Zr–O3″	70.74(14)	O3–Zr–O4	89.13(12)
O2′–Cu–O5′	78.54(15)	O4–Ti–O4′	76.63(15)	O1′–Zr–O4	113.50(13)	O3′–Zr–O5	112.98(16)
O2–Cu–O2′	101.18(15)	O4–Ti–O4″	145.2(2)	O1–Zr–O4	114.54(13)	O3–Zr–O5	73.74(15)
O2–Cu–O5	78.05(16)	O4′–Ti–O4″	76.44(15)	O1–Zr–O5	76.96(16)	O4–Zr–O5	162.62(14)
O2–Cu–O5′	179.46(13)	O4–Ti–O5	101.4(2)	O2–Zr–O3	154.00(14)		
O5–Cu–O5′	102.23(16)	O5–Ti–O4″	103.2(2)	O2–Zr–O3′	96.34(16)		

ments in the **a** direction. Conversely, sharp $h\,k\,0$ reflections imply displacements || **c**. If both types of displacement coexist, reflections in both planes of reciprocal space can retain sharp profiles in a powder diffraction pattern if $0\,k\,l$ reflections are broadened only in the **a*** direction while $h\,k\,0$ reflections are broadened only parallel to **c***, since such streaking has little effect on 2θ. Hence, the structural modulation that leaves $0\,k\,l$ sharp is associated with streaking || **c*** for $h \neq 0$, and is a transverse shear on (001) polarised || **a**. Conversely, the modulation leaving $h\,k\,0$ sharp is a transverse modulation on (100) polarised || **c**. Both are consistent with shear of the structure to give a monoclinic β angle $\neq 90^\circ$. This modulation clearly deserves future study by transmission electron microscope, since it is uncertain at present whether the peak broadening is due to a continuous modulation such as the "tweed" texture seen in minerals such as potassium feldspars [25,26] and cordierite [27], twinning of a monoclinic structure, or intergrowth of a separate monoclinic phase with the orthorhombic structure.

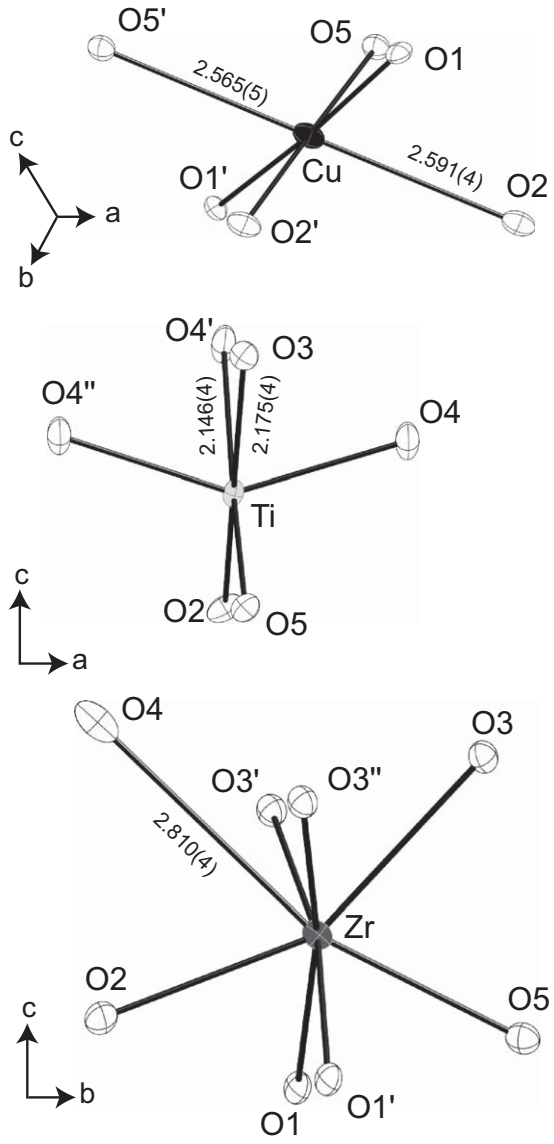

Fig. 5. Coordination environments of Cu, Ti and Zr.

3.5. Comparison to In_2TiO_5 structure

The only previously known compounds that are nearly isostructural to $CuZrTiO_5$ are In_2TiO_5 and In_2VO_5 [14,15]. These compounds are orthorhombic and have similar unit cell dimensions to $CuZrTiO_5$, but are centrosymmetric. Their space group is *Pnma*, but the axial setting corresponding to that of this study has non-standard space group symbol *Pmnb*, and for In_2TiO_5 has a=3.5018(3) Å, b=7.2418(7) Å, and c=14.890(2) Å (Fig. 7). The compound of this study could be made isostructural with In_2TiO_5 by small displacements of all atoms parallel to **a**, so as to move them onto potential mirror planes at x=0 or 1/2. The magnitudes of these displacements are 0.25–0.36 Å for the oxygens, 0.09 Å for Zr, 0.04 Å for Ti but only 0.0014 Å for Cu. These displacements change the bonding topology. In In_2TiO_5, all cations are octahedrally coordinated by oxygen. The next two closest oxygen neighbours to the Zr analogue site, In1, are at 3.005 and 3.105 Å, corresponding to bond valences of 0.04–0.05. Two oxygens are only 3-coordinated, O1 by Ti+2In2, O5 by 3Ti (oxygen sites correspond respectively to O5 and O4 of this study). The InO_6 polyhedra form 4-wide edge-sharing ribbons, elongated along **b** and packed together in a herringbone pattern. The ribbons are linked through corners to each other and zigzag chains of edge-sharing TiO_6 (Fig. 7). In $CuZrTiO_5$, the In1 site is occupied by Zr, and the In2 site by Cu (Fig. 4). Because of the cation ordering and the changes in coordination number, the herringbone pattern of octahedral ribbons is less obvious than in In_2TiO_5, and the $CuZrTiO_5$ structure instead gives the appearance of being layered || (001), consistent with the observed cleavage.

The BVS mismatch for In_2TiO_5 is even worse than for $CuZrTiO_5$, (Table 7, Column 2). The distortion patterns for all cation coordination polyhedra are different in the two structures. In addition to the removal of two oxygens from the In1 coordination polyhedron relative to Zr, In2 shows (5+1) coordination rather than the (4+2) of Cu. The Ti coordination in the indium compound is (3+3) rather than (4+2). As in $CuZrTiO_5$, the most overbonded oxygen is that which is bonded to 3 Ti, and off-centering of Ti in its coordination octahedron tends to reduce this overbonding as well as to reduce Ti⋯Ti repulsion (shortest Ti⋯Ti is only 3.301 Å in In_2TiO_5 and 3.165 Å in $CuZrTiO_5$). However, the displacement is towards an octahedral apex in In_2TiO_5 , rather than edge as in $CuZrTiO_5$ (Fig. 8), which appears to be a consequence of the additional weak bond between Zr and O4, resulting in additional

Table 6
Anisotropic displacement parameters U^{ij} (in A^2) of $CuZrTiO_5$.

	U^{11}	U^{22}	U^{33}	U^{23}	U^{13}	U^{12}
Cu	0.0139(4)	0.0071(3)	0.0102(3)	−0.0013(2)	−0.0029(3)	0.0014(2)
Zr	0.0056(2)	0.0082(2)	0.0076(2)	−0.00129(19)	−0.00022(19)	0.0003(2)
Ti	0.0047(4)	0.0065(4)	0.0080(4)	−0.0005(3)	0.0008(3)	−0.0002(4)
O1	0.0102(17)	0.0056(15)	0.0097(16)	0.0010(14)	0.0017(15)	−0.0017(19)
O2	0.014(2)	0.0092(19)	0.0094(18)	0.0009(14)	−0.0045(16)	0.0006(18)
O3	0.0092(19)	0.0074(17)	0.0093(17)	−0.0008(13)	−0.0004(16)	−0.0006(17)
O4	0.0062(19)	0.017(2)	0.0151(19)	−0.0082(16)	−0.0007(16)	0.000(2)
O5	0.009(2)	0.0104(18)	0.0087(17)	−0.0011(14)	0.0015(17)	0.0004(16)

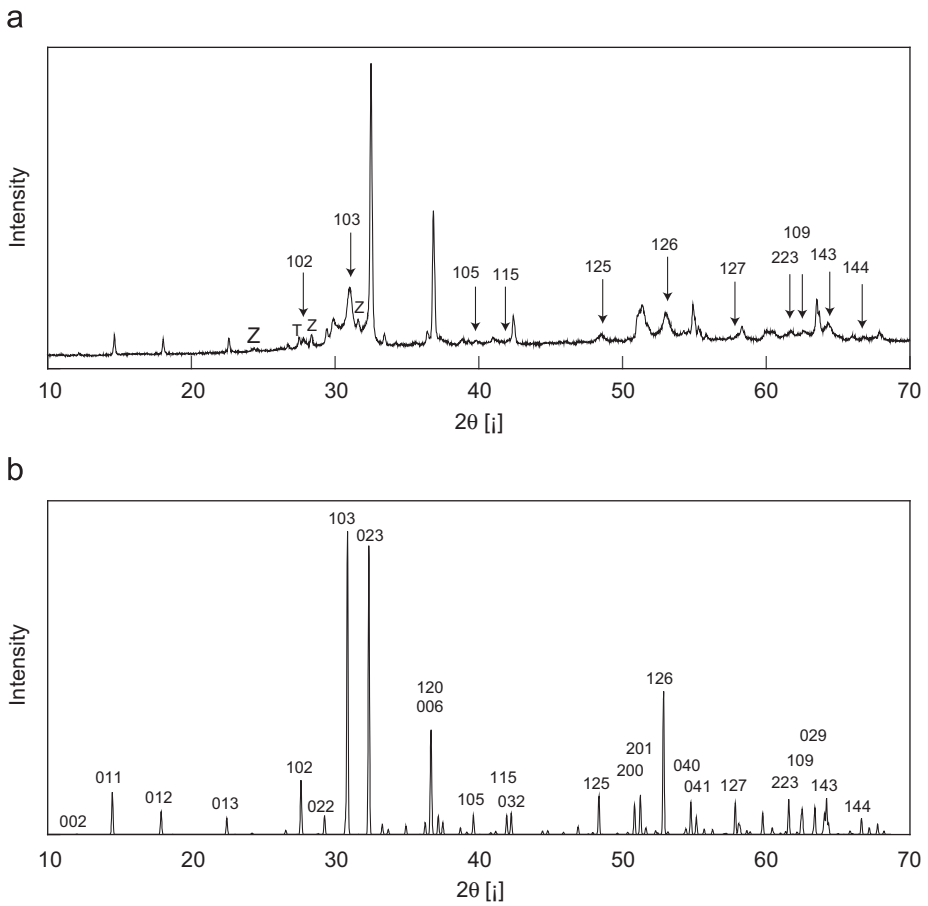

Fig. 6. (a) Experimental X-ray powder diffraction pattern for $CuZrTiO_5$. 'Z' indicates peaks from ZrO_2 impurity, 'T' indicates peaks from TiO_2 and (b) pattern calculated from single-crystal data.

shared edges of TiO_6 with ZrO_8 polyhedra and a need for Ti to avoid close approaches to Zr as well as other Ti.

In order to ascertain the reason for loss of centrosymmetry in $CuZrTiO_5$, a model structure was considered in which the x coordinates of all atoms were rounded to 0 or 1/2, so as to place them on the mirror planes of space group *Pmnb*. Bond valence calculations for this model are presented in Column 3 of Table 7. The overall BVS mismatch is worse than for the experimental structure, given that the situations of Ti and Zr are not improved and Cu is now underbonded. Furthermore, note that the Jahn–Teller elongation of the Cu octahedron is lost, since the two O2–Cu–O5 triplets are related by the mirror plane. Hence, the Cu–O coordination has changed from (4+2) to (2+4). This implies that ordering of the long Cu–O bonds is the main cause of symmetry loss.

We note above that there is X-ray powder diffraction and electron diffraction evidence for a sheared, monoclinic variant of the structure, with a, b and layer spacing $c\sin\beta$ similar to the orthorhombic structure but $\beta \neq 90^\circ$. The corresponding shear and associated relaxations may provide another mechanism for relaxing away from the bond-mismatched state, but further discussion must await more data on the nature of the monoclinic distortion.

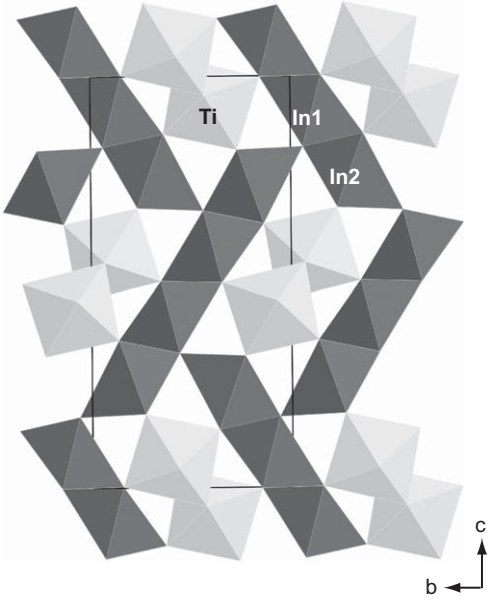

Fig. 7. Polyhedral diagram of In_2TiO_5 structure viewed down [100]. Compare $CuZrTiO_5$ in Fig. 4b.

4. Conclusions

A new inorganic compound, $CuZrTiO_5$, was synthesized, and its synthesis temperature for reaction from the oxides bracketed to 995–1010 °C. The determination of the crystal structure of $CuZrTiO_5$ showed it to be a new crystal structure type that is very similar to the structure of In_2TiO_5 and In_2VO_5, but differs from them in space group, cation coordination, and polyhedral distortion. Loss of centrosymmetry in is driven by the Jahn–Teller

Table 7
Comparison of bond valences for $CuZrTiO_5$, In_2TiO_5 and centrosymmetric model $CuZrTiO_5$.

	$CuZrTiO_5$	In_2TiO_5	$CuZrTiO_5$ *Pmnb* model
BVS[a]			
Cu (In2)	2.01	2.51	1.82
Ti	4.31	4.46	4.31
Zr (In1)	3.71	2.89	3.72
O1 (O4)	1.91	1.89	1.90
O2 (O3)	1.98	1.86	1.88
O3 (O2)	1.92	1.85	1.92
O4 (O5)	2.18	2.21	2.18
O5 (O1)	2.05	1.97	1.96
RMS Devn[b]	0.1696	0.2674	0.1855
Bond valences			
Cu-O1	0.53	0.48	0.53
Cu-O1′	0.52	0.53	0.52
Cu-O2	0.09	0.34	0.19
Cu-O2′	0.39	0.34	0.19
Cu-O5	0.40	0.42	0.20
Cu-O5′	0.09	0.11	0.20
Ti-O2	0.92	0.40	0.92
Ti-O3	0.38	0.51	0.38
Ti-O4	0.83	0.95	0.84
Ti-O4′	0.41	0.30	0.41
Ti-O4"	0.85	0.95	0.84
Ti-O5	0.93	1.15	0.93
Zr-O1	0.45	0.44	0.43
Zr-O1′	0.41	0.44	0.43
Zr-O2	0.59	0.58	0.59
Zr-O3	0.54	0.46	0.54
Zr-O3′	0.55	0.44	0.54
Zr-O3″	0.45	0.44	0.45
Zr-O4	0.09	0.04	0.09
Zr-O5	0.64	0.05	0.64

[a] BVS: bond valence sum for atom.
[b] RMS Devn: root-mean-square deviation of all BVS from their ideal values. Alternative site labelling from In_2TiO_5 refinement is shown in parentheses.

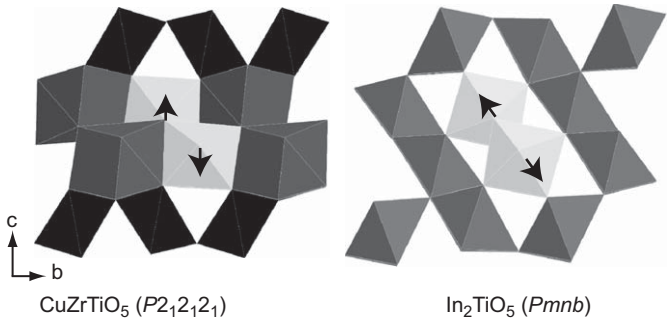

Fig. 8. Off-centering of Ti atoms from their polyhedra in $CuZrTiO_5$ (left) and In_2TiO_5 (right), showing different displacement directions due to edge-sharing ZrO_8 polyhedra in $CuZrTiO_5$.

distortion of the CuO_6 polyhedron. The structure of $CuZrTiO_5$ is characterized by significantly non-ideal bond valence sums, which seems to be due to competition between achieving ideal cation–oxygen bond lengths on the one hand, and minimising next-nearest neighbour repulsions on the other. Spatially inhomogeneous monoclinic distortion may both help to alleviate the bond valence mismatch, but the intrinsically strained nature of the structure probably contributes to its restricted temperature range of stability.

Acknowledgments

This work has been supported by Australian Research Council Discovery Project Grant DP 0559055 to David J. Ellis and Andrew G. Christy.

Appendix A. Supplementary material

Supplementary data associated with this article can be found in the online version at doi:10.1016/j.jssc.2010.01.005.

References

[1] R.E. Newnham, J. Am. Ceram. Soc. 50 (1967) 216.
[2] A. Willgallis, E. Siegmann, T. Hettiaratchi, Am. Mineral. 69 (1984) 212.
[3] G. Wilson, F. Glasser, Br. Ceram. Trans. J. 88 (1989) 69–74.
[4] U. Troitzsch, A.G. Christy, D.J. Ellis, J. Am. Ceram. Soc. 87 (2004) 2058–2063.
[5] U. Troitzsch, D.J. Ellis, J. Mater. Sci. 40 (2005) 4571–4577.
[6] U. Troitzsch, D.J. Ellis, Eur. J. Mineral. 16 (2004) 577–584.
[7] U. Troitzsch, A.G. Christy, D.J. Ellis, J. Solid State Chem. 180 (2007) 2885–2895.
[8] U. Troitzsch, J. Am. Ceram. Soc. 89 (2006) 3201–3210.
[9] Z. Otwinowski, W. Minor, Methods Enzymol., Macromol. Crystallogr. Part A 276 (1997) 307–326.
[10] A. Altomare, G. Cascarano, C. Giacovazzo, A. Guagliardi, M.C. Burla, G. Polidori, M. Camalli, J. Appl. Crystallogr. 27 (1994) 435–436.
[11] P.W. Betteridge, J.R. Carruthers, R.I. Cooper, K. Prout, D.J. Watkin, J. Appl. Crystallogr. 36 (2003) 1487.
[12] D. Hennings, J. Solid State Chem. 31 (1980) 275–279.
[13] Inorganic Crystal Structure Database, Fachinformationszentrum Karlsruhe, ⟨http://icsdweb.fiz-karlsruhe.de/⟩, 2007.
[14] P.J. Senegas, J.-P. Manaud, J. Galy, Acta Crystallogr. B 31 (1975) 1614–1618.
[15] T. Gaewdang, J.P. Chaminade, P. Gravereau, A. Garcia, C. Fouassier, P. Hagenmuller, R. Mahiou, Mater. Res. Bull. 28 (1993) 1051–1060.
[16] G. Teufer, Acta Crystallogr. 15 (1962) 1187.
[17] J. Barrett, Introduction to Atomic and Molecular Structure, Wiley, Bristol, 1970.
[18] P. Niggli, Zeitschr. Kristallogr., Kristallgeom., Kristallphys., Kristallchem. 57 (1922) 253–299.
[19] S. Benmokhtar, H. Belmal, A. El Jazouli, J.P. Chaminade, P. Gravereau, S. Pechev, J.C. Grenier, G. Villeneuve, D. de Waal, J. Solid State Chem. 180 (2007) 772–779.
[20] M. Kunz, I.D. Brown, J. Solid State Chem. 115 (1995) 395–406.
[21] M. O'Keeffe, Structure and Bonding 71 (1989) 161–190.
[22] I.D. Brown, The Chemical Bond in Inorganic Chemistry: The Bond Valence Model, IUCr Monographs on Crystallography, vol. 12, Oxford University Press, 2002 270 pp.
[23] N.E. Brese, M. O'Keeffe, Acta Crystallogr. B 47 (1991) 192–197.
[24] D.M. Adams, A.G. Christy, J. Haines, M. Clark S, Phys. Rev. B 46 (1992) 11358–11367.
[25] J.D.C. McConnell, Phil. Mag. 11 (1965) 1289–1301.
[26] R.A. Eggleton, P.R. Buseck, Contrib. Miner. Petrol. 74 (1980) 123–133.
[27] A. Putnis, S.A.T. Redfern, C.A. Fyfe, H. Strobl, Phys. Chem. Miner. 14 (1987) 446–454.